

Resonant transmission of scalar waves through rotating traversable wormhole

Rajesh Karmakar,^{1,*} Bum-Hoon Lee,^{2,3,1,†} and Wonwoo Lee^{2,‡}

¹*Department of Physics, Shanghai University, 99 Shangda Road, Shanghai, 200444, China*

²*Center for Quantum Spacetime, Sogang University, Seoul 04107, Korea*

³*Department of Physics, Sogang University, Seoul 04107, Korea*

The viability of traversable wormholes as exotic compact objects requires the identification of signatures that distinguish them from other compact objects. Given recent advances in observing rotating black hole signatures, identifying characteristic imprints that reflect the absence of an event horizon and the presence of a throat structure is of considerable significance. Motivated by this, in the present work, we analyze the propagation of a massless scalar field in a rotating traversable wormhole spacetime described by Teo's class of solutions. We numerically compute the transmission (greybody) factor and the corresponding absorption spectrum across a broad range of frequencies. The spectrum exhibits a series of sharp peaks in the amplitudes, which we identify as Breit–Wigner–type resonances. The emergence of such peaks can be attributed to the scalar modes temporarily trapped within the potential well formed by barriers on either side of the throat. These resonant features, previously identified in static wormhole backgrounds, persist in the rotating case. In particular, for Teo's class of wormholes, we find that rotation enhances the strength of the resonances. Overall, our results demonstrate the role of rotation in shaping the resonance effect and indicate these features as characteristic signatures of wormhole geometries.

I. INTRODUCTION

The Universe is undergoing dynamic evolution, with its primary energy budget consisting of time-evolving dark energy and dark matter. Consequently, investigations on the solutions that coexist with matter fields, along with the vacuum solutions to the Einstein equations, will continue to be of profound interest. Over the past decade, there has been significant progress in probing the strong-field regime of gravity through gravitational-wave detections and observations of black hole (BH) shadow images. However, these measurements are primarily sensitive up to the photon sphere, leaving open the possibility that exotic compact objects may exist alongside vacuum BH solutions [1, 2].

Wormholes (WHs) are extraordinary solutions that go beyond the vacuum solution allowed by general relativity. Einstein and Rosen were the first to conduct a serious study of WH physics, considering a bridge connecting two identical sheets of spacetime [3]. This object has been extensively studied alongside its various physical properties [4–6] and has gained modern revitalization with the work of Morris and Thorne [7]. Their proposal initiated the traversable scenario through a WH, in a more or less geometric setting. However, it has been pointed out that traversability requires exotic matter to prevent the throat from collapsing. In contrast to the usual gravitating matter, this leads to the violation of the null energy condition [8–11]. Firstly, even before the Morris-Thorne proposal, it was shown that a phantom-

like scalar field with negative kinetic energy can support the traversable WH [5]. Subsequently, extensions involving charged scalar fields resulting in charged WHs have been developed [12–17]. The concept of ‘charge without charge’ has been introduced in Ref. [4] and its geometric realization has been explored [18–21]. Although a large amount of literature is devoted to the investigation of spherically symmetric spacetimes (see [22] for an extensive discussion), a simultaneous effort has also led to the development of axisymmetric and generically asymmetric WH geometries [23–25].

Of particular importance in the present work are rotating axis-symmetric WHs, which carry several motivations. Astrophysically, most compact objects are rotating, which makes the inclusion of angular momentum essential for realistic models. In fact, rotation has been shown to improve the stability of WH spacetimes [26]. In contrast to the static case, the presence of rotation sometimes also reduces the violation of the null energy condition [27, 28]. From an observational perspective, rotating WHs may support accretion disks, whose properties could differ from those around rotating BHs, providing potential signatures to distinguish between the two [29–31].

Without explicit construction, Teo proposed a rotating scenario, extending the Morris-Thorne-type traversable WH, completely based on the symmetry arguments [32]. Later, the possibility of a source term for such a rotating WH spacetime has been studied [33]. Afterwards, several axis-symmetric WHs have been proposed [27, 34–36]. Although observable signatures of such WH geometries have not yet been detected, a range of scenarios regarding their existence have been explored, along with studies of their potential astrophysical implications [37–45].

In this paper, we study the propagation of a minimally

* rajesh@shu.edu.cn

† bhl@sogang.ac.kr

‡ warrior@sogang.ac.kr

coupled scalar test field in the background of a rotating traversable WH given by the Teo metric [32]. We compute the associated reflection and transmission coefficients and use them to determine the absorption cross section (ACS). The scattering and absorption properties of WH spacetimes, particularly in the static case, have been investigated in previous works, where they were shown to exhibit distinctive features compared to those of BHs [46–48]. In particular, quasibound states localized near the throat have been shown to appear as narrow resonant peaks in the absorption spectrum. These characteristics may provide insight into the accretion processes of such exotic compact objects.

For the simplification of the discussion, we consider the scalar field to be massless. Additionally, it is assumed that such a field does not backreact or simply does not hamper the sensitive geometry of the WH. With similar considerations, the absence of superradiance phenomena for rotating WH spacetime has been previously pointed out in [49]. In the same paper, the authors also computed the reflection and transmission coefficients for the static WH case. However, to the best of our knowledge, a similar study in the case of a rotating WH spacetime has not yet been carried out. Importantly, the bosonic waves in the low-frequency regime exhibit superradiant amplification for rotating BHs. In the absence of such phenomena in the WH case, it is imperative and interesting to investigate the impact of rotations, particularly in the low-frequency regime, where the two compact objects should differ.

The remainder of the paper is organized as follows. In Section II, we briefly discuss the rotating traversable WH spacetime as proposed by Teo. In Section III, the governing equations have been derived for a minimally coupled massless scalar field. In Section III A, the absence of superradiance phenomena is explained, and the greybody factor is defined. In Section III B, the normalization factor of the scalar wave making an arbitrary angle of incidence with the spin axis has been derived. Subsequently, in Section III C, the ACS was defined, and the results for the partial and total ACS were analyzed. Finally, in Section IV, we have concluded with the future outlook of the present work.

II. BRIEF DISCUSSION OF TEO-CLASS WORMHOLES

The class of WH solutions introduced by Teo [32] constitutes a generalization of the Morris–Thorne traversable WHs, extending them from a static spherically symmetric configuration to a stationary axially symmetric framework. The associated spacetime metric, in its original form as proposed by Teo, is expressed

as

$$ds^2 = -N^2 dt^2 + \frac{dr^2}{\left(1 - \frac{b}{r}\right)} + r^2 K^2 \left[d\theta^2 + \sin^2 \theta (d\varphi - \Omega dt)^2 \right], \quad (1)$$

where the four functions N, b, K and Ω are generally dependent on (r, θ) . The geometry of the WH is primarily encoded in the shape function $b(r, \theta)$, which sets the position of the throat. From the shape function expressed in the Morris-Thorne-type form [7], the position of the throat can be easily identified by the *apparent singularity* at $r = b$. However, the lapse function N , which represents the gravitational redshift, must remain finite and nonzero throughout the domain, to ensure traversability. In the angular part, the metric function K is regular, positive, and non-decreasing, in the sense that $\partial_r R > 0$, with $R = rK$ denoting the proper radial distance. Whereas, the rotation is governed by the function Ω , which represents the angular velocity of the WH. Furthermore, to ensure that the metric is non-singular on the rotation axis, the derivatives of N, b and K with respect to θ should vanish at $\theta = 0$ and $\theta = \pi$.

For the WH to be stable, with a traversable throat, a key geometric constraint arises from the requirement that the WH open outward at the throat. This geometry can be further analyzed by embedding an equatorial spatial slice of the WH into a Euclidean space [7]. This leads to the essential flare-out condition [50], which can be quantified as $\partial_r b < 1$ at the WH throat. When this condition is met, the metric describes two symmetric regions joined by a traversable throat at $r = b = r_0$ and $r_0 \leq r < \infty$. Additionally, demanding asymptotically flatness requires,

$$N(r) = 1 - \frac{M}{r} + \mathcal{O}\left(\frac{1}{r^2}\right), \quad \frac{b}{r} = \mathcal{O}\left(\frac{1}{r}\right), \quad (2)$$

$$K = 1 + \mathcal{O}\left(\frac{1}{r}\right), \quad \Omega = \frac{2J}{r^3} + \mathcal{O}\left(\frac{1}{r^4}\right).$$

From this, the conserved charges of the Teo WHs can be identified as M and J , corresponding to the ADM mass and angular momentum, respectively. Nevertheless, the existence of a stable and traversable throat necessarily entails the violation of the null energy condition (NEC). While this requirement was originally established for asymptotically flat, static, and spherically symmetric WHs [7], it has since been shown to persist irrespective of asymptotic or global properties, as well as in more general, non-symmetric configurations [51]. For the present case of Teo WHs, the constraints imposed on the metric functions, as outlined so far, are sufficient to ensure that the NEC is violated near the throat [32].

Maintaining the essential characteristics of the Teo WH spacetime, and motivated by phenomenological considerations [52–54], we adopt the following parameteriza-

tion of the metric functions.

$$b(r) = r_0, \quad N = e^{-r_0/r}, \quad \Omega = \frac{2J}{r^3}, \quad K = 1, \quad (3)$$

where r_0 is a constant in which the flare-out condition [7, 50, 55] is satisfied for $r_0 > 0$. Whereas, the angular momentum of the WH J is related to the dimensionless spin parameter, a ,¹ via $a \equiv J/M^2$. Importantly, $a = 0$ yields the static version of the traversable WH spacetime. Nevertheless, in the rest of the analysis, therefore, we will follow the line element of (1) with the metric functions given above in (3). Within this setup, our main objective is to study how a test scalar field propagates within this rotating background with a traversable throat at r_0 .

III. A TEST SCALAR FIELD MINIMALLY COUPLED WITH THE WORMHOLE SPACETIME

On the background of the rotating traversable WH spacetime, outlined in the previous section, we consider a minimally coupled massless test scalar field, described by the following action:

$$A = -\frac{1}{2} \int \sqrt{-g} d^4x \partial_\mu \phi \partial^\mu \phi, \quad (4)$$

where g represents the determinant of the spacetime metric (1), explicitly, $\sqrt{-g} = r^2 N(r) \sin \theta / (1 - r_0/r)$ (3). Given the above action, the equation of motion of the scalar field reads

$$\partial_\mu (\sqrt{-g} g^{\mu\nu} \partial_\nu \phi) = 0. \quad (5)$$

For the rotating traversable WH solution under consideration, the governing equation of the scalar field can be expressed as

$$\begin{aligned} & -\frac{1}{N(r)^2} (\partial_t + \Omega(r) \partial_\varphi)^2 \phi \\ & + \frac{\sqrt{1 - \frac{r_0}{r}}}{r^2 N(r)} \partial_r \left(r^2 N(r) \sqrt{1 - \frac{r_0}{r}} \partial_r \phi \right) \\ & + \frac{1}{r^2 \sin^2 \theta} \partial_\varphi^2 \phi + \frac{1}{r^2 \sin \theta} \partial_\theta (\sin \theta \partial_\theta \phi) = 0. \end{aligned} \quad (6)$$

Let us decompose the field into spherical harmonics as

$$\phi = \sum_{lm} \mathcal{N}_{\omega lm} e^{-i\omega t} R_{lm}(r) Y_{lm}(\theta, \varphi), \quad (7)$$

with $\mathcal{N}_{\omega lm}$ denoting the overall normalization constant, which will be fixed in later sections. Here, ω represents

¹ The dimensional relationship between the rotation parameter in the Kerr BH geometry, \mathbf{a} , and the dimensionless spin parameter in this geometry is given by $[\mathbf{a}] = [aM]$.

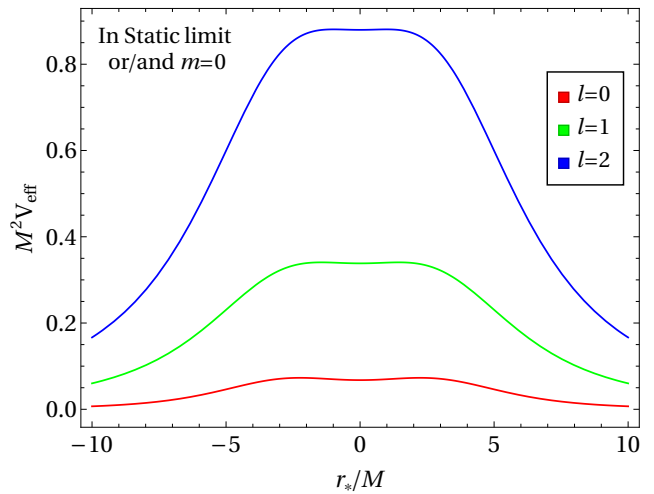


FIG. 1. Effective potential of the scalar field in the static limit of the WH, $a = 0$, or/and for azimuthal mode, $m = 0$.

the frequency of the scalar field, while l and m represent the orbital angular momentum number and the magnetic number, respectively. The modes with $m > 0$ are corotating with the WH, while those with $m < 0$ are counterrotating. Notably, for rotating BH geometry [56], one usually get the decoupled angular equation to result in spheroidal harmonics. In the special class of Teo WH, we find that spherical harmonics suitably decouple the equation of motion. Nevertheless, with such a decomposition, the equation of motion of the unknown radial part turns out as²

$$\begin{aligned} & \frac{1}{r^2 N(r)} \sqrt{1 - \frac{r_0}{r}} \frac{d}{dr} \left(r^2 N(r) \sqrt{1 - \frac{r_0}{r}} \frac{dR_{lm}}{dr} \right) \\ & + \left[\frac{(\omega - m \Omega(r))^2}{N(r)^2} - \frac{l(l+1)}{r^2} \right] R_{lm}(r) = 0. \end{aligned} \quad (8)$$

Moving forward, we find it suitable to utilize the Tortoise coordinate, defined as $dr_*/dr = 1 / (N(r) \sqrt{1 - r_0/r})$, which smoothly connects both sides of the WH through the throat. Particularly, for $r_0 \leq r < \infty$, the Tortoise radial coordinate ranges over $-\infty < r_* < \infty$, with $r_* \rightarrow 0$ as $r \rightarrow r_0$. We also find it convenient to rescale the radial part of the scalar field in the following manner

$$R(r) \equiv \frac{u(r)}{r}. \quad (9)$$

² The present WH geometry has the vanishing $T_{r\theta}$ component of the energy-momentum tensor. Furthermore, its metric form resembles that of a slowly rotating Kerr BH, and it may possess a Killing tensor [57] associated with Carter's constant [58]. This means that it can be considered a geometry with a separability structure [59, 60]. Consequently, separation of variables is possible for the scalar field equation in this geometry [61].

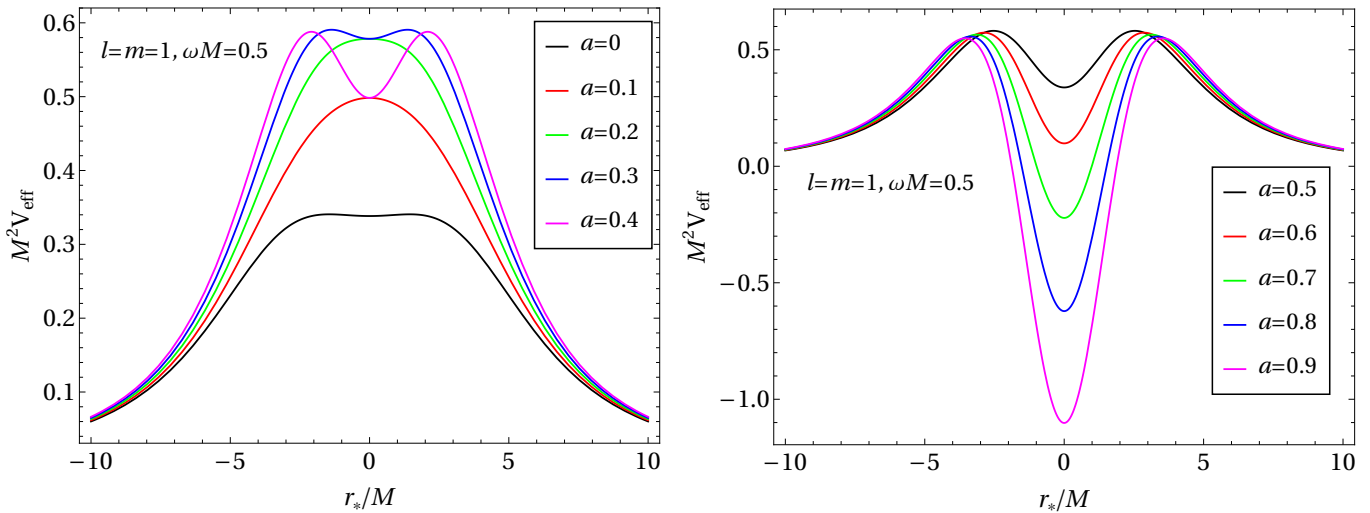


FIG. 2. The effective potential barrier for the scalar field has been plotted with r_*/M . In the **left panel**, variations for different values of the spin parameter in the lower range are shown, while in the **right panel**, variations for different values of the spin parameter in the higher range are presented. For plots in both panels, the frequency, orbital and azimuthal mode numbers have been kept fixed.

Then, the radial equation reduces to a Schrödinger-like form

$$\frac{d^2 u}{dr_*^2} + [\omega^2 - V_{\text{eff}}(r)] u = 0, \quad (10)$$

where the effective potential is given by

$$V_{\text{eff}}(r) = 2m\omega\Omega(r) - m^2\Omega(r)^2 + N^2(r) \left[\frac{l(l+1)}{r^2} + \frac{\sqrt{1-\frac{r_0}{r}}}{rN(r)} \frac{d}{dr} \left(N(r) \sqrt{1-\frac{r_0}{r}} \right) \right]. \quad (11)$$

This definition of the effective potential captures most of the parameter dependence of the scattering states of the scalar field quite well. In the static case $a = 0$, as illustrated in Fig. 1, the height of the effective potential barrier increases monotonically with orbital mode l . Looking more closely, one can identify a shallow potential well bounded by barriers on both sides of the WH throat. However, as the value of l increases, the well disappears. Previous studies have demonstrated that the presence of a well in the effective potential leads to trapped modes, which may manifest as resonance peaks in the transmission spectrum of static WHs, such as the generalized Ellis–Bronnikov [46] and the Simpson–Visser spacetime [47].

As the spin of the WH increases, shown in the left panel of Fig. 2, potential wells begin to emerge more clearly. For sufficiently high spin, they develop into a pronounced potential well-type structure as illustrated in the right panel of Fig. 2. Particularly, the double barrier emerges due to the symmetry of the WH spacetime on both sides of the WH throat. On top of it,

having the rotation in spacetime, the frequency and the azimuthal mode together play a significant role, as has been shown in Fig. 3. Importantly, we find that the co-rotating modes, characterized by positive azimuthal mode m , exhibit only a shallow well as compared to the counter-rotating ones, with negative m , for smaller values of the spin, although the well becomes significantly deeper as the spin increases. Whereas the scalar modes with $m = 0$ do not feel the effects of rotation, and the effective potential also becomes independent of the frequency. In the following discussion, we will see how the scattering states of the scalar field behave due to the effective potential bearing the above characteristics.

A. Greybody factor for the scalar field

In the asymptotic limits ($r_* \rightarrow \pm\infty$), the effective potential tends to vanish with respect to the frequency of the scalar field (see (10) and (11)) due to the asymptotic flatness of the present class of WH spacetime. Hence, asymptotic radial solutions become superpositions of plane waves. To study the scattering process by the BH spacetime, one needs to impose the boundary conditions such that the scalar wave is purely ingoing near the horizon and a superposition of ingoing and outgoing near special infinity [62]. In contrast, the presence of a traversable throat in the WH spacetime leads the wave to be purely ingoing near $r_* \rightarrow -\infty$ [47, 49]. With this in mind, the asymptotic solutions can be expressed in the following manner:

$$u(r) = \begin{cases} \mathcal{I}_{\omega lm} e^{-i\omega r_*} + \mathcal{R}_{\omega lm} e^{i\omega r_*}, & r_* \rightarrow \infty, \\ \mathcal{T}_{\omega lm} e^{-i\omega r_*}, & r_* \rightarrow -\infty, \end{cases} \quad (12)$$

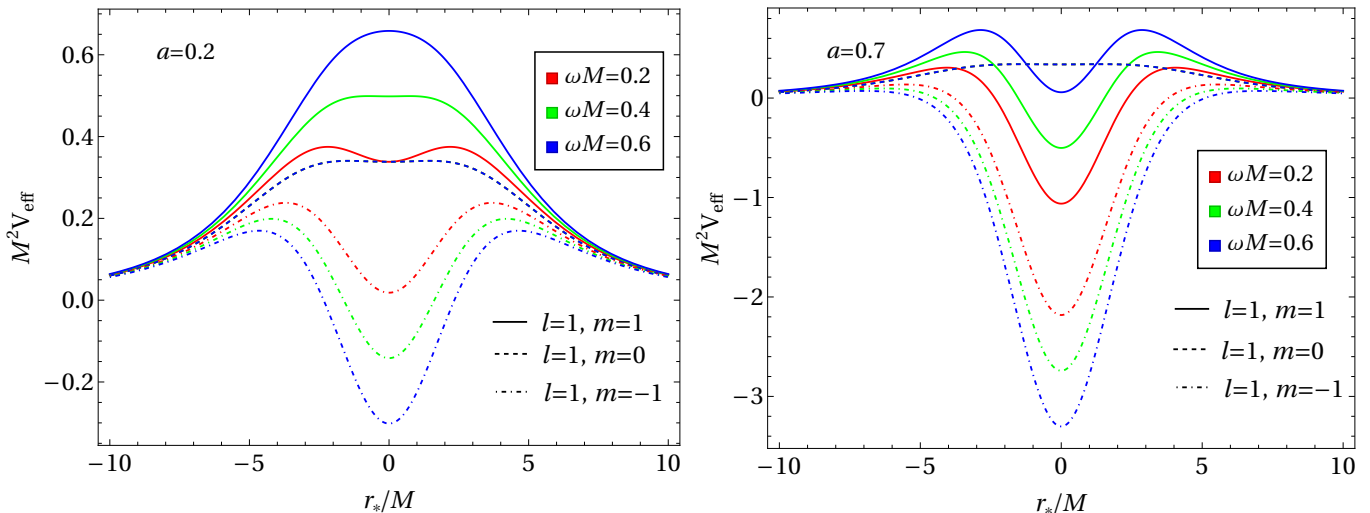


FIG. 3. The effective potential barrier for the scalar field has been plotted with r_*/M . In the **left panel**, variations corresponding to different values of the scalar field frequency are shown (in different colors), along with the consideration of different azimuthal mode, $m = 1$ (solid line), $m = 0$ (dashed line) and $m = -1$ (dot-dashed line) for a fixed orbital modes, $l = 1$, given a fixed value of the spin parameter of the WH, $a = 0.3$. In the **right panel**, similar variations have been considered, however, for a higher value of the spin parameter, $a = 0.7$, of the WH.

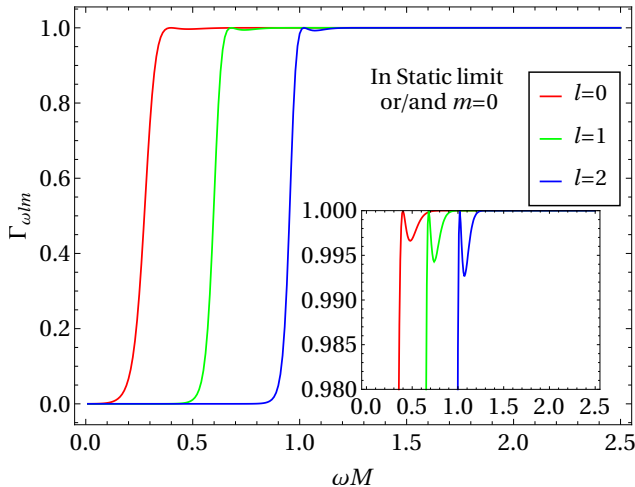


FIG. 4. Greybody factor for the scalar field in the static limit of the WH, $a = 0$, or/and for azimuthal mode, $m = 0$. The inset figure demonstrates the enlarged version before the greybody factor saturates to unity, where the appearance of resonance peaks can be seen.

where $\mathcal{I}_{\omega lm}$, $\mathcal{R}_{\omega lm}$ and $\mathcal{T}_{\omega lm}$ represent the incident, reflection, and transmission coefficients, respectively. Whereas, $e^{i\omega r_*}$ denotes the outgoing mode, while $e^{-i\omega r_*}$ denotes the ingoing mode, with the temporal part given in (7). The conserved Wronskian associated with the linear second-order differential equation (10), $W[u, u^*] =$

$u\partial_{r_*}u^* - u^*\partial_{r_*}u$, turns out to be

$$W[u, u^*] = \begin{cases} 2i\omega(|\mathcal{I}_{\omega lm}|^2 - |\mathcal{R}_{\omega lm}|^2), & r_* \rightarrow \infty, \\ 2i\omega|\mathcal{T}_{\omega lm}|^2, & r_* \rightarrow -\infty. \end{cases} \quad (13)$$

Then the conservation of the Wronskian leads to the following condition based on the above equation,

$$(|\mathcal{I}_{\omega lm}|^2 - |\mathcal{R}_{\omega lm}|^2) = |\mathcal{T}_{\omega lm}|^2. \quad (14)$$

This condition implies the absence of superradiance phenomena in the WH spacetime, even in the presence of rotation, which is in contrast to the usual rotating BH spacetime. In a traversable WH, any negative-energy component generated inside the ergoregion is not irreversibly lost behind a horizon, unlike in a BH spacetime [63]. Instead, the wave can propagate through the throat and emerge into the other asymptotic region [49]. The incident wave will be partly reflected and partly transmitted at the throat without any amplification. Nevertheless, in this scenario, one can suitably define the greybody factor, accounting for the transmission of the matter field [64], to study the scattering phenomena, as

$$\Gamma_{\omega lm} = 1 - \left| \frac{\mathcal{R}_{\omega lm}}{\mathcal{I}_{\omega lm}} \right|^2 = \frac{|\mathcal{T}_{\omega lm}|^2}{|\mathcal{I}_{\omega lm}|^2}. \quad (15)$$

Therefore, the greybody factor represents the probability that an incident wave will successfully cross the potential barrier and through the throat of a WH. In what follows, we will outline the procedure for computing the reflection and transmission coefficients numerically, which will determine the greybody factor, as defined above.

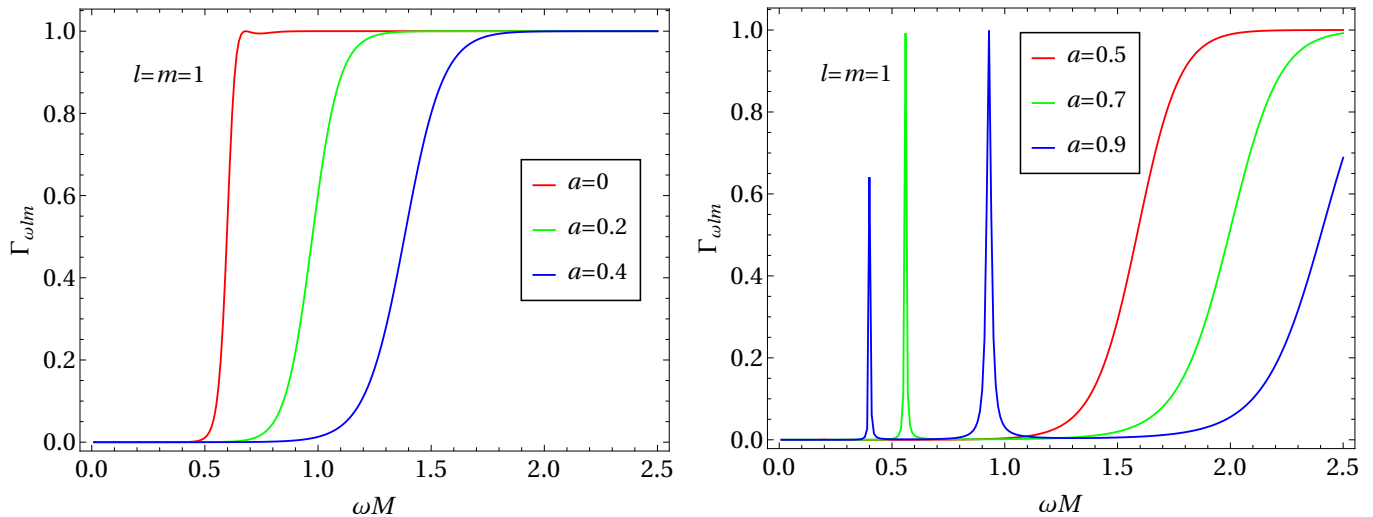


FIG. 5. Greybody factor for the scalar field has been plotted with the frequency ωM . In the **right panel**, variations have been shown for different values of the WH spin in the lower range. In the **right panel**, the behaviour is shown for higher spin.

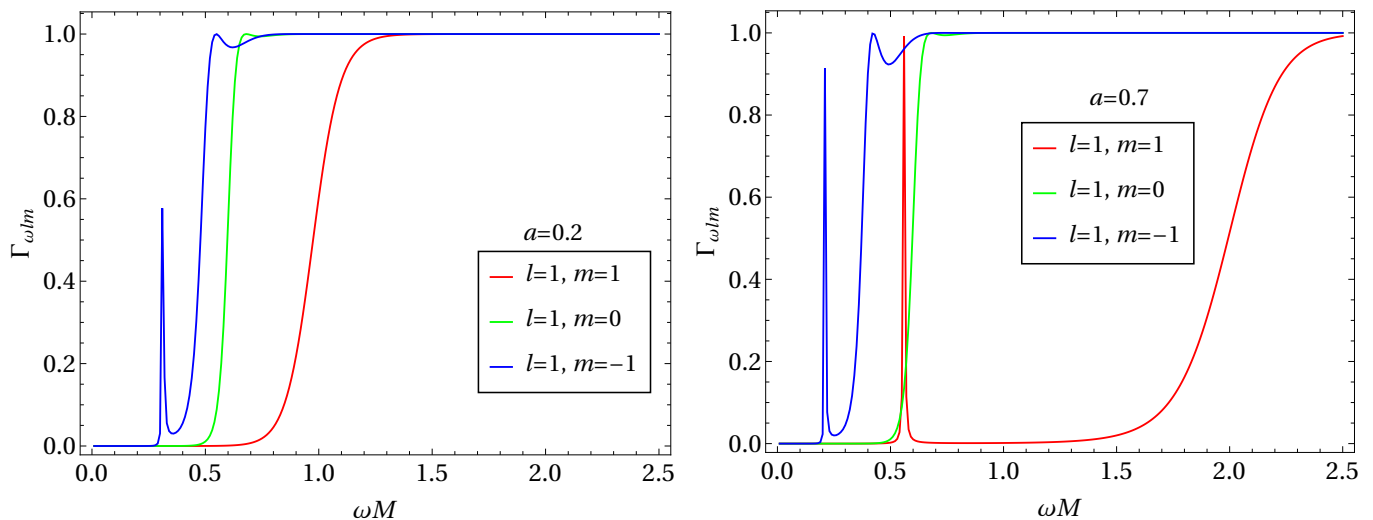


FIG. 6. Greybody factor for the scalar field has been plotted with the frequency ωM . Variations have been shown for different azimuthal modes, m , corresponding to a fixed orbital mode $l = 1$.

Numerical recipe: Although in a rotating BH space-time, the reflection and transmission coefficients can be analytically determined in the low- and high-frequency limit [56, 62], we find it simpler to deduce these coefficients numerically in the presence of the double barrier potential, and perform the analysis for arbitrary frequencies. For this purpose, the master equation (10) governing the scalar field is solved in Mathematica using the built-in NDSolve function, setting the ingoing initial condition near negative spatial infinity, explicitly, $r_{*-\infty} = -100M$. To solve the linear second-order differential equation, two conditions are needed, for which we choose the derivative of the field at $r_{*-\infty} = -100M$ to provide another initial condition. It is important to

note that this condition is not an independent condition and carries the same ingoing requirement. Therefore, the set of boundary conditions altogether reads $[u(r), u'(r)]_{r_* \rightarrow -\infty}$, which can be straightforwardly deduced from (12). Then the numerical solution is obtained at $r_\infty = 100M$, i.e., far from the WH throat. The stability of the solution is checked by varying the accuracy and precision goals available in Mathematica. Once the solution is obtained, it is then matched to the asymptotic form of the ansatz (12), and consequently, the reflection and incident coefficients are also numerically determined. Afterwards, substituting these coefficients in the above definition, the greybody factor was numerically evaluated. We should also mention that the Mathematica

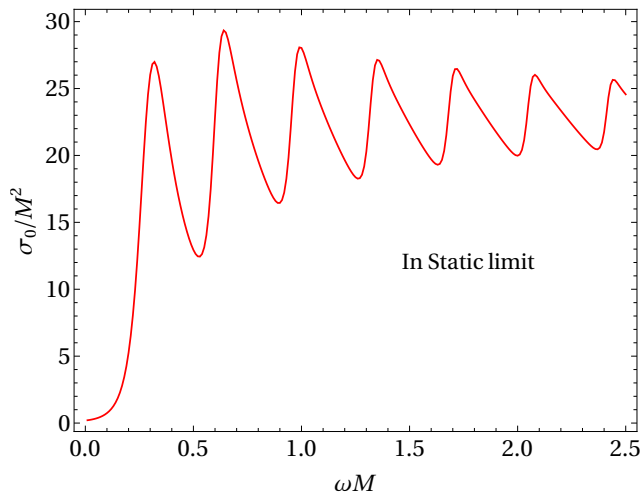


FIG. 7. Total ACS for the scalar has been plotted considering the static limit of the WH.

code developed for this purpose successfully reproduces the existing results for scattering in the case of static WH [48].

The Teo’s WH in the absence of rotation, as mentioned before, boils down to the form of a Morris-Thorne-type traversable WH. In this limiting case, the appearance of a shallow well in the effective potential for the massless scalar field has been discussed in the previous section. In Fig. 4, we have illustrated the behavior of the greybody factor for this case. The distinctive characteristic of resonant transmission can be seen for different orbital modes l , before the corresponding greybody factors saturate to the maximum value, $\Gamma = 1$. The resonance occurs for a certain frequency for each orbital mode, which can be understood following the effective potential, for example, with $\omega M \simeq 0.5$, for $l = 0$, the value of $\omega^2 M^2$ cuts through the double peak of the potential well (see Fig. 1) and makes the traveling wave outside the potential barrier to be temporarily trapped as it falls in the shallow well. These trapped modes are often referred to as quasi-bound modes [65]. Notably, they are not true bound states, given a finite barrier height, such modes spend a finite amount of time before tunnelling through the potential barrier [66]. Inside the potential well, these modes undergo repeated reflections between the adjacent barriers. Whereas phase coherence among partially reflected waves leads to constructive interference, resulting in enhanced transmission through the potential barrier. This enhancement effect is known as the Breit–Wigner-type resonance [47, 65].

Once rotation is introduced in the WH spacetime, the resonant transmission becomes more pronounced and depends on the azimuthal mode, m . Therefore, we first present the behaviour of the greybody factor for co-rotating modes, $l = 1, m = 1$, in Fig. 5. Interestingly, the resonant transmission, although has been present in

a slight manner in the static case, does not occur for this mode until $a \simeq 0.6$. This closely follows from the behaviour of the frequency-dependent effective potential for WH spin in the lower range (see Fig. 2), where a slight increase in the spin away from $a = 0$ leads to the disappearance of the potential well structure. The well then re-emerges at $a = 0.3$. However, for resonant transmission, the scalar mode should be bounded by the barrier, $\omega^2 < V_{\text{eff}}$, and should remain as travelling waves inside the well, $\omega^2 > V_{\text{eff}}$. Such a scenario is viable for higher spin for the co-rotating modes (see the right panel of Fig. 2), therefore resonant peaks are appearing in the right panel of Fig. 5. For the lower-spin, one might expect that resonant transmission could be achieved by increasing the frequency; however, as shown in Fig. 3, for $l = 1, m = 1$ the barrier height increases with frequency, thereby suppressing the possibility of resonant transmission.

For a fixed orbital mode, $l = 1$, the behaviour of the greybody factor for different azimuthal modes, m , is presented in Fig. 6. We see that the resonant transmission always happens for the counter-rotating modes (negative m) as the rotation lowers the corresponding effective potential much more efficiently (11). The resonant features can be understood in a similar manner as above, in terms of the corresponding effective potential. Importantly, for all the above cases, the frequencies at which the resonant peaks appear should, in principle, be closely related to long-lived quasinormal modes [47, 65]. Given the complexity involved in computing quasinormal modes for a rotating traversable WH, which gives rise to a double-peak potential barrier, we leave this analysis for future work. In the present work, we have discussed how such long-lived modes can be identified directly from the transmission spectra and interpreted through the corresponding effective potential barrier. For example, from Fig. 6, we identify prominent resonant frequencies at $\omega M \sim 0.32$ and $\omega M \sim 0.22$ for $a = 0.2$ and $a = 0.7$, respectively, in the case $l = 1, m = -1$, while for $l = 1, m = 1$ we find $\omega M \sim 0.54$ for $a = 0.7$. These frequencies are expected to be associated with the real part of the imaginary component of long-lived QNMs, as discussed in Ref. [48]. Nevertheless, in the following analysis, the greybody factor will be further used to compute the ACS. For this purpose, the scalar field should be normalized first.

B. Normalization of the scalar field

To keep the present analysis on a general footing, the incoming massless scalar wave is considered to have an incident angle with the WH spin axis γ . However, the Rayleigh expansion provides for the decomposition of a plane wave in terms of partial waves, which can be ex-

pressed as [67],

$$e^{-i\omega(t+r\cos\theta')} = \sum_l (2l+1)i^l e^{-i\omega t} j_l(\omega r) P_l(\cos\theta'), \quad (16)$$

with

$$\cos\theta' = \cos\gamma\cos\theta + \sin\gamma\sin\theta\cos\phi, \quad (17)$$

where $j_l(\omega r)$ represents the spherical Bessel function and $P_l(\cos\theta')$ denotes the Legendre function [68]. Whereas θ' stands for the projected WH angular coordinate with the incident angle, so that,

$$P_l(\cos\theta') = \frac{4\pi}{2l+1} \sum_{m=-l}^l Y_{lm}(\theta, \varphi) Y_{lm}^*(\gamma, 0). \quad (18)$$

With the above setup, the incident plane wave expression now becomes

$$e^{-i\omega(t+r\cos\theta')} = - \sum_l 2\pi i \frac{e^{-i\omega(t+r)}}{\omega r} Y_{lm}(\theta, \varphi) Y_{lm}^*(\gamma, 0), \quad (19)$$

where we have used the fact that for $r \rightarrow \infty$ or $\omega r \gg 1$, the asymptotic form of the spherical Bessel function reads

$$j_l(\omega r) \sim i^{l+1} \frac{e^{-i\omega r}}{2\omega r} + (-i)^{l+1} \frac{e^{i\omega r}}{2\omega r}. \quad (20)$$

Utilizing the asymptotic form of the radial solution at spatial infinity (12), the asymptotic form of the scalar field (7) can be expressed as

$$\phi = \sum_{lm} \mathcal{N}_{\omega lm} \left[\mathcal{I}_{\omega lm} \frac{e^{-i\omega(t+r)}}{r} + \mathcal{R}_{\omega lm} \frac{e^{-i\omega(t-r)}}{r} \right] Y_{lm}(\theta, \varphi). \quad (21)$$

By matching this asymptotic form with (19), the overall normalization constant is determined to be

$$\mathcal{N}_{\omega lm} = -i \frac{2\pi}{\omega \mathcal{I}_{\omega lm}} Y_{lm}^*(\gamma, 0). \quad (22)$$

In the next section, this normalization factor will be utilized to determine the total and partial ACS of the WH for the scalar field.

C. Absorption cross section for the scalar field

The energy flux measured by a static observer (as Teo's WH is asymptotically static) at $r \rightarrow \infty$, per unit time is

$$\partial_t \mathcal{E} = \int d\Omega r^2 \mathcal{T}_{tr}, \quad (23)$$

where for a massless scalar field the stress energy tensor $\mathcal{T}_{\mu\nu}$ is given by

$$\mathcal{T}_{\mu\nu} = \frac{1}{2} (\partial_\mu \phi^* \partial_\nu \phi + \partial_\mu \phi \partial_\nu \phi^*) - \frac{1}{2} g_{\mu\nu} \partial^\alpha \phi^* \partial_\alpha \phi. \quad (24)$$

Substituting the asymptotic form of the massless scalar field solution (21)

$$\partial_t \mathcal{E} = \int d\Omega r^2 \mathcal{T}_{tr} = \sum_l |\mathcal{N}_{\omega lm}|^2 \omega^2 (|\mathcal{I}|^2 - |\mathcal{R}|^2). \quad (25)$$

The ACS is defined by taking the ratio of the above energy flux rate to the incident energy density [69], which happens to be $2\omega^2$, so that

$$\sigma = \frac{\partial_t \mathcal{E}}{2\omega^2}. \quad (26)$$

Including the expression of the normalization factor from (22), the final expression of the ACS reads

$$\sigma = \frac{4\pi^2}{\omega^2} \sum_{lm} |Y_{lm}(\gamma, 0)|^2 \Gamma_{\omega lm}. \quad (27)$$

For the on-axis incidence, i.e., $\gamma = 0$, the above expression becomes

$$\sigma_0 = \frac{\pi}{\omega^2} \sum_{lm} (2l+1) \delta_{m0} \Gamma_{\omega lm}. \quad (28)$$

Having discussed the numerical procedure for computing the greybody factor in Section III A, it is now straightforward to evaluate the partial and total ACS of the WH for the scalar field. It is evident from the above discussion that the partial ACS differs from the greybody factor for individual modes only by an overall multiplicative factor. Hence, the features discussed before for the greybody factor directly carry over to the ACS. Therefore, in what follows, we present only the total ACS of the WH, which should exhibit non-trivial features.

In Fig. 7, the total ACS for the scalar field is illustrated in the static limit of the WH, i.e., in the absence of rotation in the spacetime. Owing to the shallow potential barrier in this case, a small increase in the amplitudes can be observed in the low-frequency regime, as opposed to the more regular oscillations around the saturated geometric capture cross section seen in the case of BH spacetimes [62]. A very similar result was obtained a long time ago for a generalized Ellis-Bronnikov WH spacetime [46]. Moreover, since the spin parameter appears together with the azimuthal mode in the equation of motion (10), for incidence along the axis the ACS does not depend on the rotation of the WH spacetime, which is again in contrast to the usual rotating BH case [62].

Because of the rotation, the spectrum is expected to depend strongly on the angle at which the incident wave approaches the WH throat relative to its spin axis. In Fig. 8, we have shown the behaviour of the total ACS for the rotating scenario for off-axis incidence. We find that the amplitude of the resonance, particularly in the lower range of the frequency, increases and becomes sharper with the increase in the rotation. This is in accordance with the fact that the corresponding effective potential

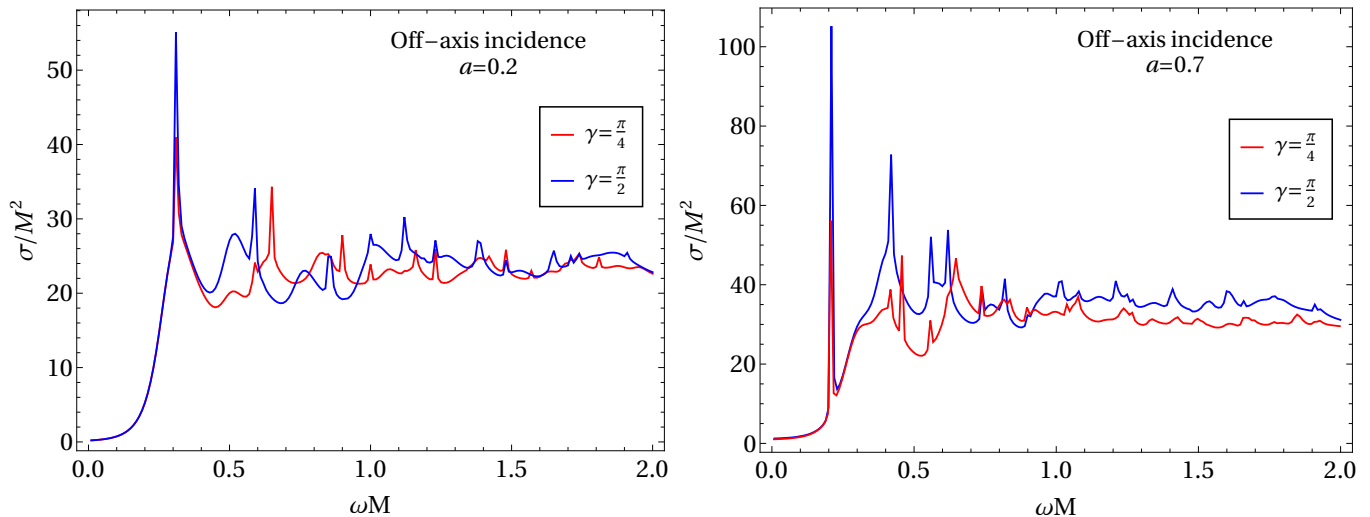


FIG. 8. Total ACS of the WH has been plotted with respect to the frequency of the scalar field. **In the left panel:** We have considered smaller values for the spin parameter, $a = 0.2$, whereas, **in the right panel** a higher value, $a = 0.7$, has been chosen.

has a deeper cavity well structure as compared to the static case. The low-frequency regime is particularly relevant for the resonant behaviour, as the scalar modes should be trapped inside the well. Otherwise, they will be transmitted without resonance. The spectrum also exhibits stronger resonance with the increase in the incident angle from the rotation axis, and the maximum effect is found for the perpendicular incidence. In the next section, we summarize the overall features and their significance.

IV. CONCLUSION AND OUTLOOK

We have discussed how rotation in the traversable WH spacetime leads to prominent, sharp peaks at different frequencies in the absorption spectrum of a massless scalar field. Because of the rotation, the spectrum is expected to depend strongly on the angle at which the incident wave approaches the WH throat relative to its spin axis. However, given the special structure of the present Teo-class WHs, the angular momentum appears in a specific manner, due to which on-axis incidence also corresponds to the static limit. As a result, the scalar wave does not feel the rotation in such a situation. This is in contrast to the case of rotating Kerr BHs [56].

In the static limit, which is also analogous to the case of on-axis incidence, we do not observe any pronounced resonance peaks in the absorption spectrum. Importantly, it was previously found for static Simpson–Visser WHs [48], and more generally for static clean photon-sphere objects (ClePhOs) [65], belonging to the class of exotic compact objects, that sharp resonance peaks already appear in this static case due to a prominent cavity in the

effective potential. However, the static geometry for the present Teo-class WHs differs from these objects, particularly near the throat, and the cavity well in the effective potential appears to be shallow, as has also been encountered in [46, 49, 70].

With the inclusion of rotation in the WH spacetime, the effective potential exhibits a deep-cavity structure. Specifically, this happens efficiently for counter-rotating modes. Consequently, the resonance amplitude, particularly at lower frequencies, increases and becomes sharper. Therefore, in contrast to superradiance phenomena in rotating BH [63], we find resonant transmission to be a distinguishable feature for rotating WH in the low-frequency regime. The spectrum also exhibits stronger resonance with the increase in the incident angle from the rotation axis, and the maximum effect is found for the perpendicular incidence. Evidently, such an angle-dependent cross-section, absent in the case of static WH [46, 48], could be relevant as far as the observation is concerned.

As a final remark, it is important to note that we have adopted a specific Teo-class WH due to its simplicity and its ability to provide a generic framework for a rotating WH geometry. Within the Teo class, a variety of configurations can be explored [53]. However, for models that differ solely in the choice of redshift function, while preserving the remaining metric properties, such as asymptotic flatness and the rotational features of the present class, the conclusions of this work are not expected to change. Over the years, several other classes of rotating traversable WHs have been put forward [36, 71, 72], which merit further investigation to develop a comprehensive understanding of their distinguishing signatures and how they may be distinguished from their BH counterparts. In this regard, the present analysis provides a

useful basis for such investigations.

ACKNOWLEDGEMENTS

RK thanks the research group of Xian-Hui Ge for the useful discussions held during the weekly meetings at the Physics Department of Shanghai University. RK is also grateful to Debaprasad Maity for numerous discussions over the years on scattering phenomena in curved

backgrounds in general. BHL was supported by the National Research Foundation of Korea (NRF) (RS-2026-25473640 and RS-2024-00339204) and by Overseas Visiting Fellow Program of Shanghai University. BHL would like to thank the hospitality of the KIAS and APCTP during the visit where a part of this work has been done. WL was supported by RS-2026-25484780, BHL and WL were also supported by Basic Science Research Program of the National Research Foundation of Korea funded by the Ministry of Education through CQUeST (RS-2020-NR049598).

-
- [1] R. Abbott *et al.* (LIGO Scientific, VIRGO, KAGRA), Phys. Rev. D **112**, 084080 (2025), arXiv:2112.06861 [gr-qc].
- [2] S. Vagnozzi *et al.*, Class. Quant. Grav. **40**, 165007 (2023), arXiv:2205.07787 [gr-qc].
- [3] A. Einstein and N. Rosen, Phys. Rev. **48**, 73 (1935).
- [4] C. W. Misner and J. A. Wheeler, Annals Phys. **2**, 525 (1957).
- [5] H. G. Ellis, J. Math. Phys. **14**, 104 (1973).
- [6] L. Chetouani and G. Clément, Gen. Rel. Grav. **16**, 111 (1984).
- [7] M. S. Morris and K. S. Thorne, Am. J. Phys. **56**, 395 (1988).
- [8] F. S. N. Lobo, Phys. Rev. D **71**, 084011 (2005), arXiv:gr-qc/0502099.
- [9] F. S. N. Lobo and D. Rubiera-Garcia, in *15th Marcel Grossmann Meeting on Recent Developments in Theoretical and Experimental General Relativity, Astrophysics, and Relativistic Field Theories* (2020) arXiv:2008.09902 [gr-qc].
- [10] M. S. Churilova, R. A. Konoplya, Z. Stuchlík, and A. Zhidenko, JCAP **10**, 010 (2021), arXiv:2107.05977 [gr-qc].
- [11] G. Antoniou, A. Bakopoulos, P. Kanti, B. Kleihaus, and J. Kunz, Phys. Rev. D **101**, 024033 (2020), arXiv:1904.13091 [hep-th].
- [12] H. Huang and J. Yang, Phys. Rev. D **100**, 124063 (2019), arXiv:1909.04603 [gr-qc].
- [13] N. Godani and G. C. Samanta, Phys. Scripta **96**, 015303 (2021).
- [14] Y. Koga, R. Maeda, D. Saito, K. Uemichi, and D. Yoshida, Phys. Rev. D **113**, 044035 (2026), arXiv:2505.20040 [gr-qc].
- [15] F. Rahaman, A. Aziz, T. Manna, A. Islam, N. A. Pundeer, and S. Islam, J. Korean Phys. Soc. **86**, 1204 (2025).
- [16] B. Turimov, A. Abdujabbarov, B. Ahmedov, and Z. Stuchlík, Phys. Lett. B **868**, 139800 (2025).
- [17] J. L. Blázquez-Salcedo, L. M. González-Romero, F. S. Khoo, J. Kunz, and P. Navarro Moreno, (2025), arXiv:2510.11406 [gr-qc].
- [18] S.-W. Kim and H. Lee, Phys. Rev. D **63**, 064014 (2001), arXiv:gr-qc/0102077.
- [19] H.-C. Kim, S.-W. Kim, B.-H. Lee, and W. Lee, J. Korean Phys. Soc. **88**, 401 (2026), arXiv:2405.10013 [gr-qc].
- [20] H.-C. Kim and W. Lee, (2025), arXiv:2505.09981 [gr-qc].
- [21] V. Dzhunushaliev and V. Folomeev, (2025), arXiv:2512.00958 [gr-qc].
- [22] M. Visser, *Lorentzian wormholes: From Einstein to Hawking* (1995).
- [23] C. Hoffmann, T. Ioannidou, S. Kahlen, B. Kleihaus, and J. Kunz, Phys. Rev. D **97**, 124019 (2018), arXiv:1803.11044 [gr-qc].
- [24] S. D. Forghani, S. Habib Mazharimousavi, and M. Halilsoy, Eur. Phys. J. C **78**, 469 (2018), arXiv:1801.05516 [gr-qc].
- [25] S. D. Forghani, S. Habib Mazharimousavi, and M. Halilsoy, JCAP **10**, 067 (2019), arXiv:1807.05080 [gr-qc].
- [26] B. Azad, J. L. Blázquez-Salcedo, F. S. Khoo, and J. Kunz, Phys. Lett. B **848**, 138349 (2024), arXiv:2301.05243 [gr-qc].
- [27] P. E. Kashargin and S. V. Sushkov, Phys. Rev. D **78**, 064071 (2008), arXiv:0809.1923 [gr-qc].
- [28] K. Uemichi, Y. Koga, D. Saito, C.-M. Yoo, and D. Yoshida, (2026), arXiv:2603.12748 [gr-qc].
- [29] T. Harko, Z. Kovacs, and F. S. N. Lobo, Phys. Rev. D **79**, 064001 (2009), arXiv:0901.3926 [gr-qc].
- [30] R. K. Karimov, R. N. Izmailov, and K. K. Nandi, Eur. Phys. J. C **79**, 952 (2019), arXiv:1901.05762 [gr-qc].
- [31] S. Paul, R. Shaikh, P. Banerjee, and T. Sarkar, JCAP **03**, 055 (2020), arXiv:1911.05525 [gr-qc].
- [32] E. Teo, Phys. Rev. D **58**, 024014 (1998), arXiv:gr-qc/9803098.
- [33] S. E. Perez Bergliaffa and K. E. Hibberd, (2000), arXiv:gr-qc/0006041.
- [34] P. Kashargin and S. Sushkov, Physical Review D—Particles, Fields, Gravitation, and Cosmology **78**, 064071 (2008).
- [35] M. S. Volkov, Phys. Rev. D **104**, 124064 (2021), arXiv:2109.14496 [gr-qc].
- [36] A. Cisterna, K. Müller, K. Pallikaris, and A. Viganò, Phys. Rev. D **108**, 024066 (2023), arXiv:2306.14541 [gr-qc].
- [37] N. Tsukamoto, T. Harada, and K. Yajima, Phys. Rev. D **86**, 104062 (2012), arXiv:1207.0047 [gr-qc].
- [38] C. Bambi, Phys. Rev. D **87**, 107501 (2013), arXiv:1304.5691 [gr-qc].
- [39] M. Azreg-Ainou, JCAP **07**, 037 (2015), arXiv:1412.8282 [gr-qc].
- [40] A. Abdujabbarov, B. Juraev, B. Ahmedov, and Z. Stuchlík, Astrophys. Space Sci. **361**, 226 (2016).

- [41] D.-C. Dai and D. Stojkovic, Phys. Rev. D **100**, 083513 (2019), arXiv:1910.00429 [gr-qc].
- [42] V. De Falco, E. Battista, S. Capozziello, and M. De Laurentis, Phys. Rev. D **101**, 104037 (2020), arXiv:2004.14849 [gr-qc].
- [43] J. H. Simonetti, M. J. Kavic, D. Minic, D. Stojkovic, and D.-C. Dai, Phys. Rev. D **104**, L081502 (2021), arXiv:2007.12184 [gr-qc].
- [44] N. Godani and G. C. Samanta, Annals Phys. **429**, 168460 (2021), arXiv:2105.08517 [gr-qc].
- [45] N. Sarkar, S. Sarkar, A. Bouzenada, A. Dutta, M. Sarkar, and F. Rahaman, Phys. Dark Univ. **44**, 101439 (2024).
- [46] S. Kar, S. Minwalla, D. Mishra, and D. Sahdev, Phys. Rev. D **51**, 1632 (1995).
- [47] H. C. D. Lima, C. L. Benone, and L. C. B. Crispino, Phys. Rev. D **101**, 124009 (2020), arXiv:2006.03967 [gr-qc].
- [48] H. C. D. Lima Junior, C. L. Benone, and L. C. B. Crispino, Eur. Phys. J. C **82**, 638 (2022), arXiv:2211.09886 [gr-qc].
- [49] R. A. Konoplya and A. Zhidenko, Phys. Rev. D **81**, 124036 (2010), arXiv:1004.1284 [hep-th].
- [50] S.-W. Kim, J. Korean Phys. Soc. **63**, 1887 (2013), arXiv:1302.3337 [gr-qc].
- [51] D. Hochberg and M. Visser, Phys. Rev. Lett. **81**, 746 (1998), arXiv:gr-qc/9802048.
- [52] P. G. Nedkova, V. K. Tinchev, and S. S. Yazadjiev, Phys. Rev. D **88**, 124019 (2013), arXiv:1307.7647 [gr-qc].
- [53] G. Gyulchev, P. Nedkova, V. Tinchev, and S. Yazadjiev, Eur. Phys. J. C **78**, 544 (2018), arXiv:1805.11591 [gr-qc].
- [54] S. Kumar, A. Uniyal, and S. Chakrabarti, Phys. Rev. D **109**, 104012 (2024), arXiv:2308.05545 [gr-qc].
- [55] D. Hochberg and M. Visser, Phys. Rev. D **56**, 4745 (1997), arXiv:gr-qc/9704082.
- [56] C. F. B. Macedo, L. C. S. Leite, E. S. Oliveira, S. R. Dolan, and L. C. B. Crispino, Phys. Rev. D **88**, 064033 (2013), arXiv:1308.0018 [gr-qc].
- [57] F. Gray and D. Kubiznak, Phys. Rev. D **105**, 064017 (2022), arXiv:2110.14671 [gr-qc].
- [58] B. Carter, Phys. Rev. **174**, 1559 (1968).
- [59] S. Benenti and M. Francaviglia, Gen. Rel. Grav. **10**, 79 (1979).
- [60] M. Demianski and M. Francaviglia, Int. J. Theor. Phys. **19**, 675 (1980).
- [61] V. P. Frolov, P. Krtous, and D. Kubiznak, JHEP **02**, 005 (2007), arXiv:hep-th/0611245.
- [62] C. L. Benone and L. C. B. Crispino, Phys. Rev. D **99**, 044009 (2019), arXiv:1901.05592 [gr-qc].
- [63] R. Brito, V. Cardoso, and P. Pani, Lect. Notes Phys. **906**, pp.1 (2015), arXiv:1501.06570 [gr-qc].
- [64] R. F. Rosato, S. Biswas, S. Chakraborty, and P. Pani, Phys. Rev. D **111**, 084051 (2025), arXiv:2501.16433 [gr-qc].
- [65] C. F. B. Macedo, T. Stratton, S. Dolan, and L. C. B. Crispino, Phys. Rev. D **98**, 104034 (2018), arXiv:1807.04762 [gr-qc].
- [66] J. J. Sakurai, S. Fu Tuan, and R. G. Newton, "Modern quantum mechanics," (1986).
- [67] W. G. Unruh, Phys. Rev. D **14**, 3251 (1976).
- [68] M. Abramowitz and I. A. Stegun, *Handbook of Mathematical Functions with Formulas, Graphs, and Mathematical Tables*, National Bureau of Standards Applied Mathematics Series, Vol. 55 (U.S. Government Printing Office, Washington, D.C., 1964) reprinted by Dover Publications, 1965.
- [69] V. Cardoso and R. Vicente, Phys. Rev. D **100**, 084001 (2019), arXiv:1906.10140 [gr-qc].
- [70] J. Riley, (2026), arXiv:2604.14238 [gr-qc].
- [71] B. Kleihaus and J. Kunz, Phys. Rev. D **90**, 121503 (2014), arXiv:1409.1503 [gr-qc].
- [72] X. Y. Chew, B. Kleihaus, and J. Kunz, Phys. Rev. D **94**, 104031 (2016), arXiv:1608.05253 [gr-qc].